ADVANCED FUNCTIONAL MATERIALS

www.afm-journal.de

Novel Safeguarding Tactile e-Skins for Monitoring Human Motion Based on SST/PDMS–AgNW–PET Hybrid Structures

Sheng Wang, Liping Gong, Zejin Shang, Li Ding, Guansheng Yin, Wanquan Jiang, Xinglong Gong, and Shouhu Xuan**

A novel versatile electrical skin (e-skin) with safeguarding and multisensing properties based on hybrid structures is developed by assembling Ag nanowires (AgNWs), polyester (PET) film with hybrid shear stiffening polymer/polydimethylsiloxane (SST/PDMS) matrix. The hybrid SST/PDMS polymer shows stable configuration. Storage modulus of the SST/PDMS increases from 5.5 kPa to 0.39 MPa when the shear frequency changes from 0.1 to 100 Hz, exhibiting typical rate-dependent behavior. e-Skin functions as a human-monitoring device by detecting various motions such as gentle touching, stroking, elbow bending, as well as speaking. More importantly, due to the shear stiffening characteristic, e-skin with high damping capacity exhibits safeguarding performance, which can dissipate impact force from 720 to 400 N and increase buffer time (from 0.9 to 2 ms). Meanwhile, distinguishable resistance values can reveal the level of harsh impact applied on the e-skin. In addition, the visible thermosensation effect of e-skin similar to chameleon epidermis is convenient for assessing environmental temperature. e-Skin arrays can precisely map the dynamic impact location and pressure distribution. Finally, the high electrical sensitivity and shear stiffening performance are attributed to the disturbance of AgNW effective conductive paths and dynamic B—O bonds, respectively.

1. Introduction

Skin, as the largest organ in human body, plays a vital role in human interaction with external surroundings by perceiving and responding to the stimuli such as pressure, heating, and moisture.[1,2] With the increasing demand of health monitoring and human–machine interaction, artificial electrical skin (e-skin) with high sensitivity, multifunctional sensing performance to mimic human skin's sensory ability has aroused significant research interest all over the world.[3,4] So far, various types of e-skins, such as piezoresistive-,[5–8] capacitive-,[9,10] triboelectric-[11,12] and piezoelectric-type[13,14] skins have been developed. Especially, piezoresistive-type e-skins, conventionally built on flexible polymer substrates and conductive nanofillers such as carbon nanotube, graphene, and conductive nanowires, enable to efficiently transduce pressure into resistance signals.[15–18] Due to easy fabrication, high sensitivity, and low cost, the piezoresistive-type sensor is a promising e-skin in monitoring pressure, strain, and human movement.[19–21]

Recently, in order to emulate functions of human skins more precisely, more great efforts have been made to develop multifunctional piezoresistive e-skins.[22] A stretchable film to mimic the self-healing and pressure-sensitive properties of nature skin was designed by integrating graphene and polymers into a thin film and the high stability enabled its potential application in artificial skins.[23] A sophisticated energy-autonomous e-skin consisting of graphene and photovoltaic cell could not only transform light to electric energy but also show sensitivity to touch pressure.[24] This novel tactile e-skin patch fixed on a prosthetic hand presented ideal stimuli-responsive properties by performing various tasks. Very recently, a sandwiched polydimethylsiloxane/single walled carbon nanotube/polydimethylsiloxane (PDMS/SWCNT/PDMS) e-skin film presented ideal responses to thermal and light radiation due to the unique tunable cracked microstructures.[25] So far, the reported e-skins with high electrical sensitivity are mainly focused on mimicking the sensing properties of human skin but have largely ignored other crucial functions. Especially, the sophisticated structures of skin also can protect human body against external damage.[26] However, to our knowledge, the investigation of e-skins with safeguarding as well as reliable sensing properties is still vacant.

Shear stiffening (SST) polymer, a derivative of silly putty, is an intelligent viscoelastic polymer whose storage modulus (G') and stiffness show orders of magnitude increment when the external

Dr. S. Wang, L. Ding, Prof. X. Gong, Prof. S. Xuan
CAS Key Laboratory of Mechanical Behavior and Design of Materials
Department of Modern Mechanics
University of Science and Technology of China (USTC)
Hefei 230027, P. R. China
E-mail: xuansh@ustc.edu.cn

L. Gong, Prof. Z. Shang, Prof. G. Yin
School of Science
Chang'an University
Xi'an 710061, P. R. China
E-mail: yings@chd.edu.cn

Prof. W. Jiang
Department of Chemistry
University of Science and Technology of China
Hefei 230026, P. R. China

DOI: 10.1002/adfm.201707538

shear frequency is beyond a critical value. The rate-dependent soft–rigidity transition and controllable damping factor (tanδ) endow its great promising application in damping, vibration and controlling as well as in protection.[27–29] A smart wearable Kevlar-based electronic textile combining with SST polymer showed 190% increment in anti-impact force than neat Kevlar fabrics.[30] Silly putty with the performance of reversibly switching from "liquid" to "solid" could act as an intelligent dynamic protection surface for the stable operation and uniform deposition/stripping of Li metal electrodes.[31] Additionally, SST polymer was also a good candidate for preparing a novel sensor with the gauge factor >500 and a quantitative model was proposed to describe the electromechanical performance.[32] However, SST polymer presents remarkable creep properties and its height collapses by 50% within 20 min which seriously limits its practical applications.[33] Therefore, SST polymer with stable configuration and conductivity may be an ideal candidate for mimicking the safeguarding and sensing properties of human skin.

In this work, a three-layered-structured e-skin with multiple sensing properties and safeguarding performance was designed by embedding Ag nanowires (AgNWs) into a sandwich construction composed of polyester (PET) film and a hybrid polymer matrix. The hybrid polymer was fabricated by mixing SST gel with small amounts of polydimethylsiloxane (PDMS). It also possesses good electrical sensitivity which can monitor external bending, compressing, twisting as well as temperature. More importantly, the reported e-skin shows shear-rate-dependent mechanical property. Due to high damping capacity, the e-skin can reduce the impact force by nearly 50%, thus presents ideal safeguarding performance. Additionally, e-skin arrays efficiently locate external dynamic loading force and pressure distribution, which show promising application in monitoring human interactions, personal movement, and safeguarding areas.

2. Results and Discussion

2.1. Fabrication of the e-Skin and Characterization of the Rate-Dependent Rheological Properties

The fabrication processes of e-skin are schematically illustrated in **Figure 1**. Briefly, SST polymer was obtained by heating the mixture of dimethyl siloxane, boric acid, and ethanol at 220 °C (Figure 1a,b). Then, blend SST polymer, High temperature vulcanized (HTV) silicone rubber, benzoyl peroxide (BPO), and thermochromic fillers by a two-roll miller. Second, the synthesized AgNWs were suspended in ethanol to form the AgNW solution (Figure 1d) and dropwise dipped on PET film to form conductive AgNW layer. Third, AgNWs/PET film was covered on the hybrid polymer composite and vulcanized at 90 °C under 20 MPa for 15 min (Figure 1f,g). Finally, the copper wire electrodes were fixed on the cooling composites to achieve the artificial e-skin (Figure 1h,i).

In this work, five different mass ratios (SST:PDMS), 100:0, 90:10, 70:30, 50:50, and 0: 100, were employed to fabricate mixture polymer with definite dimension. SST polymer shows a typical cold flow feature (**Figure 2**a) while pure PDMS is incompressible (Figure 2b). Mixed polymer with too little PDMS (the ratio of 90:10) cannot recover back after being compressed (Figure 2c), while hybrid polymer with the ratio of 70:30 exhibits stable dimension and ideal recovery property by compression (Figure 2d-I–d-III). Due to the adhesive character, SST polymer as well as hybrid polymer with the ratio of 70:30 also adheres ideally even when cut into pieces (Figure 2e-I,e-II, g-IV–g-VI). However, when the ratio of PDMS increases to 50%, the polymer shows an elastic feature, in which the pieces no longer adhere with each other (Figure 2f). To this end, the ratio of 70:30 of hybrid polymers is employed for preparation of artificial skin.

Undoubtedly, SST (Figure S1a, Supporting Information) and the hybrid polymer (**Figure 3**a) are soft and can be stretched by low rate. As for PDMS, it is stiff and brittle, which will be broken up once being stretched (Figure S1b, Supporting Information). Due to the shear stiffening effect, SST polymer can turn to stiff and absorb the energy when a harsh impact is performed (high rate, Figure 3b). Here, the hybrid polymer shows similar performance (Figure 3c). Figure 3e,f show the Fourier transform infrared (FTIR) and X-ray diffraction (XRD) patters of the polymer composites. SST and PDMS are composed of similar components from the FT-IR spectrum. However, the characteristic absorption bands located at 890 and 860 cm^{-1} indicate the formation of Si—O—B bond in SST polymer. The hybrid polymer also inherits Si—O—B bond from SST polymer which shows similar test results. The XRD pattern also presents

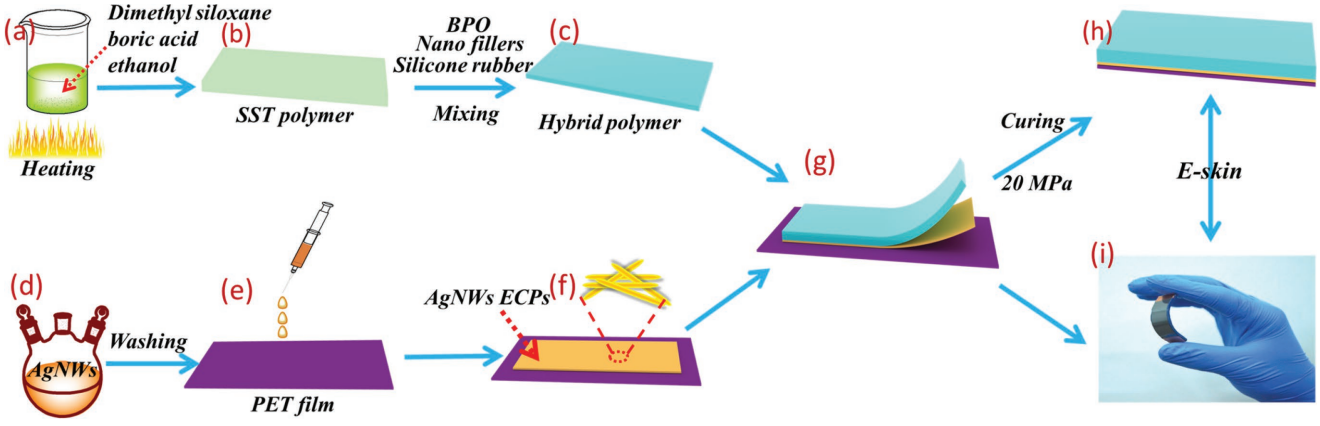

Figure 1. Schematic diagram of fabrication steps for a–c) preparing the hybrid polymer; d–f) synthesizing Ag nanowire (AgNW) effective conductive paths (ECPs); and g–i) curing the composites and the as-prepared e-skin.

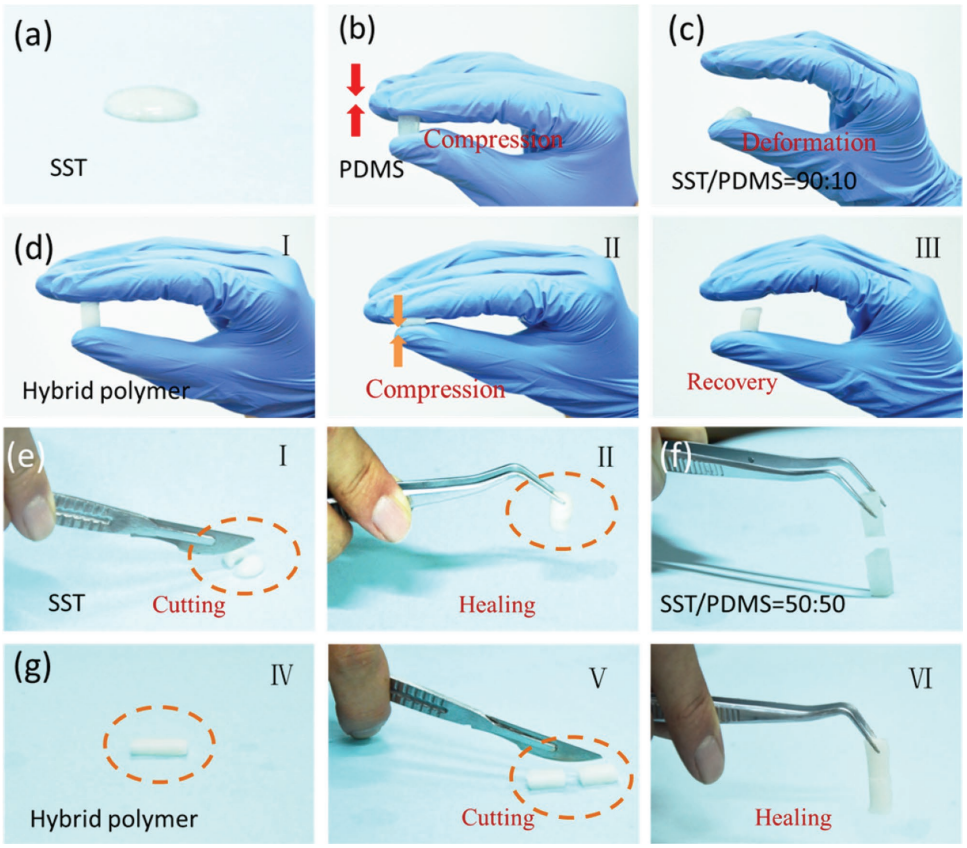

Figure 2. Schematic of the compression-recovery properties of a) shear stiffening (SST) polymer, b) polydimethylsiloxane (PDMS) , hybrid polymer (SST/PDMS) in the ratio of c) 90:10 and d-I–d-III) 70:30; healing properties of e-I,e-II) SST polymer, f) hybrid polymer (SST/PDMS = 50:50), g-IV–g-VI) and hybrid polymer in the ratio of 70: 30.

similar consequence. The three-layered e-skin contains hybrid polymer with 10 wt% of thermochromic nanofillers, AgNW layers, and PET film, to mimic the structures of human skin. AgNWs adhered on PET film to form effective conductive paths (ECPs) which endows its ideal conductivity (Figure S1c, Supporting Information). The scanning electron microscopy (SEM) images of the thermochromic nanofillers are shown in Figure S2 (Supporting Information). These spherical fillers with the diameter in the range of 1–8 µm are incorporated into the hybrid polymer (Figure S1e, Supporting Information). Rheological tests were carried out to investigate the shear rate-dependent mechanical properties of the as-prepared composites. The initial storage modulus (G'_{min}) of the plastic SST polymer at 0.1 Hz is 61.2 Pa while it increases dramatically as the external shear frequency increases and the maximum G' (G'_{max}) is as high as 0.7 MPa (100 Hz), indicating remarkable shear stiffening property. O atoms in SST polymer chains can share electrons with B atoms which form dynamic bond (similar to hydrogen bond). When shear stress is loaded under high rate, large numbers of dynamic cross bonds impede the slippage of polymer chains in short time, and the polymer shows stiff character (Figure 3d). However, B—O cross bonds have enough time to break (Figure 3d), and polymer chains can recombine with each other if the loaded force is under a low rate. Thus, the composite exhibits soft and viscoelastic properties. When 30% of PDMS is introduced, the initial G' is undoubtedly increased to 5.5 kPa and the G'_{max} is 0.39 MPa. In addition, thermochromic fillers also show positive influence on G'. The G'_{min} and G'_{max} values of artificial skin (hybrid polymer-10% in Figure 3g) are 15 kPa and 0.61 MPa, respectively, which also presents a rate-dependent feature. However, too many nanofillers can remarkably enhance the mechanical properties of the hybrid polymer. As for PDMS, G' is independent of external stimuli, and G'_{min} and G'_{max} are all 0.12 MPa. To this end, the rheological performance of the as-prepared artificial skin is ideally rate dependent which proves that the stiffness of the composite can be varied by changing external stimulus.

2.2. Monitoring Human Motions

Force sensing capability of artificial skin versus static compression is shown in **Figure 4**. e-Skin is fixed on mechanical testing system (MTS) and different pressures are loaded with simultaneously recording the electrical signals. During the loading–unloading cycles, e-skin offers a rapid response which exhibits high sensitivity. As the pressure is 1, 5, 20, and 50 N, $\Delta R/R_0$ increases from 2%, 3%, 9% to 18%, respectively (Figure 4a-I–a-IV). These dramatic responses show ideal stability; thus, it can be used to evaluate externally applied pressure. The varied response to different bending deformations is also investigated (Figure 4b). Typical variations in $\Delta R/R_0$ can be observed, and the peak values of e-skin excited by compression strains

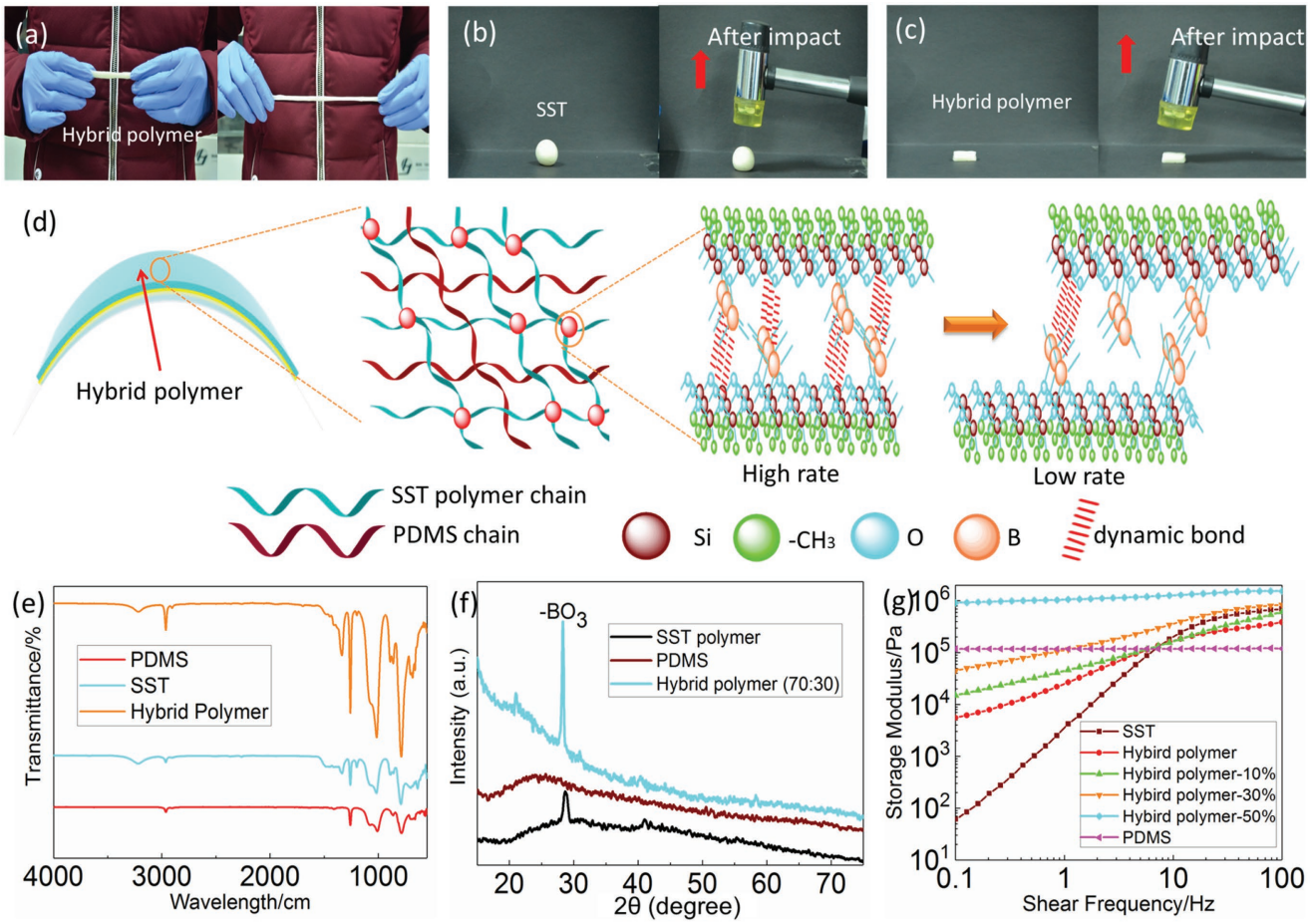

Figure 3. a) Stretchability of hybrid polymer with low extension rate. b) Anti-impact of SST and c) the hybrid polymer. Mechanism of d) shear stiffening effect, e) Fourier transform infrared (FT-IR), and f) X-ray diffraction (XRD) of the as-prepared polymer composites. g) Rate-dependent rheological properties of as-prepared polymer composites in the shear frequency of 0.1–100 Hz.

of 1%, 5%, 10%, and 30% are 5%, 12%, 18%, and 106%, respectively. The outputting signals for resistance changes are stable, and the flexural strain can be reliably assessed based on the distinguished changing values of $\Delta R/R_0$. The generated signals simulated by static compression are lower than those excited by bending and twisting, which is attributed to

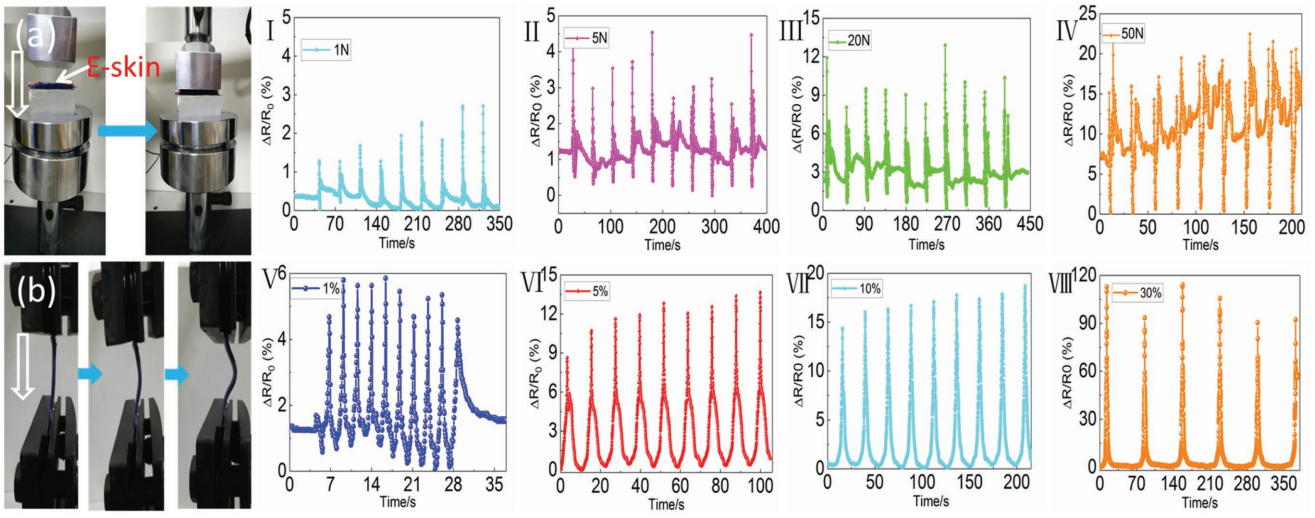

Figure 4. Force sensing performance of artificial skin simulated by different pressure: a-I–a-IV) mechanical testing system (MTS) devices 1, 5, 20, and 50 N. b) Variation of $\Delta R/R_0$ of e-skin as a function of bending strain in cycles: e-skin fixed on MTS: b-V–b-VIII) bending strains of 1%, 5%, 10%, and 30%.

the deformation of AgNW ECPs. Large amounts of AgNWs adhered on PET film can form ECPs which is beneficial for the conductivity of e-skin (Figure S3a,b, Supporting Information). Under quasistatic compression, e-skin can sustain the pressure; small microcracks appear (Figure S3c, Supporting Information); and the tight junctions between AgNWs and polymer substrate lead to lower increment in resistance.[34] However, once bent, AgNW junctions are detached, slid against each other,[35–37] and the separated ECPs lead to higher and sharper electrical signals. Additionally, parts of the bending AgNWs embedded into polymer composites are not easily back to initial positions due to the polymer friction force.[38] Thus, longer microcracks of ECPs and loose junctions between AgNWs lead to higher electrical signals under bending and twisting excitations (Figure S3d–f, Supporting Information).

Various human motions and complicated muscle movements such as gentle touching, bending, as well as speaking are measured to investigate the tactile-perception behavior of the e-skin. The artificial skin immediately responds to a gentle touch and recovers back within 5 s, indicating its excellent detection sensitivity (**Figure 5**a). However, it can sense the force by stroking and the electrical signal can maintain 70 s (Figure 5b). Undoubtedly, e-skin can distinguish external pressure and exhibit reliable stability (Figure 5c,d). Figure 5e–h further displays the application of this e-skin as a proof-of-concept vibration-pressure sensor. It can detect the vibration of throat by spelling "USTC." A high platform of $\Delta R/R_0$ at 38% lasting about 3s is attributed to the vibration of throat shouting, and this process can be repeated many times without changes in maximum value (Figure 5i). Additionally, when grasping a glass bottle, the bending finger drastically leads to an increase in resistance ($\Delta R/R_0 \approx 100\%$, Figure 5j). The e-skin attached on human elbow can also distinguish the bending and releasing process with repeated cycles (Figure 5k). The peak value of $\Delta R/R_0$ by large-scale motion (twist) increases to about 190% in Figure 5l. In conclusion, the as-prepared artificial skin with high sensitivity, excellent sensing performance, and cyclic stability presents potential applications for monitoring and analyzing human motions.

2.3. Safeguarding and Force Sensing properties

To further mimic the protection as well as tactile sensing properties of e-skin, a drop hammer test device is applied to load–unload the impact excitation. The falling heights and weights are varied according to the experiments. e-Skin with the length, width, and thickness of 40 × 15 × 3 mm is fixed on the force transducer, which is further placed on the button of a metal pedestal (**Figure 6**a). During the impact, the force sensor captures the signals and transfers to an oscilloscope. The electrical data are simultaneously saved by an electrical impedance spectroscopy (EIS) system. When the impactor contacts the target, the impact force starts to increase to a maximum value and attenuate to 0 in short time (Figure 6b). Once contact the force sensor, the impact kinetic energy (induced by impactor falling from 5 cm) is thoroughly absorbed by the metal pedestal, inducing the maximum force of 720 N. However, the maximum force loading on e-skin is dramatically decreased to 400 N, which suggests

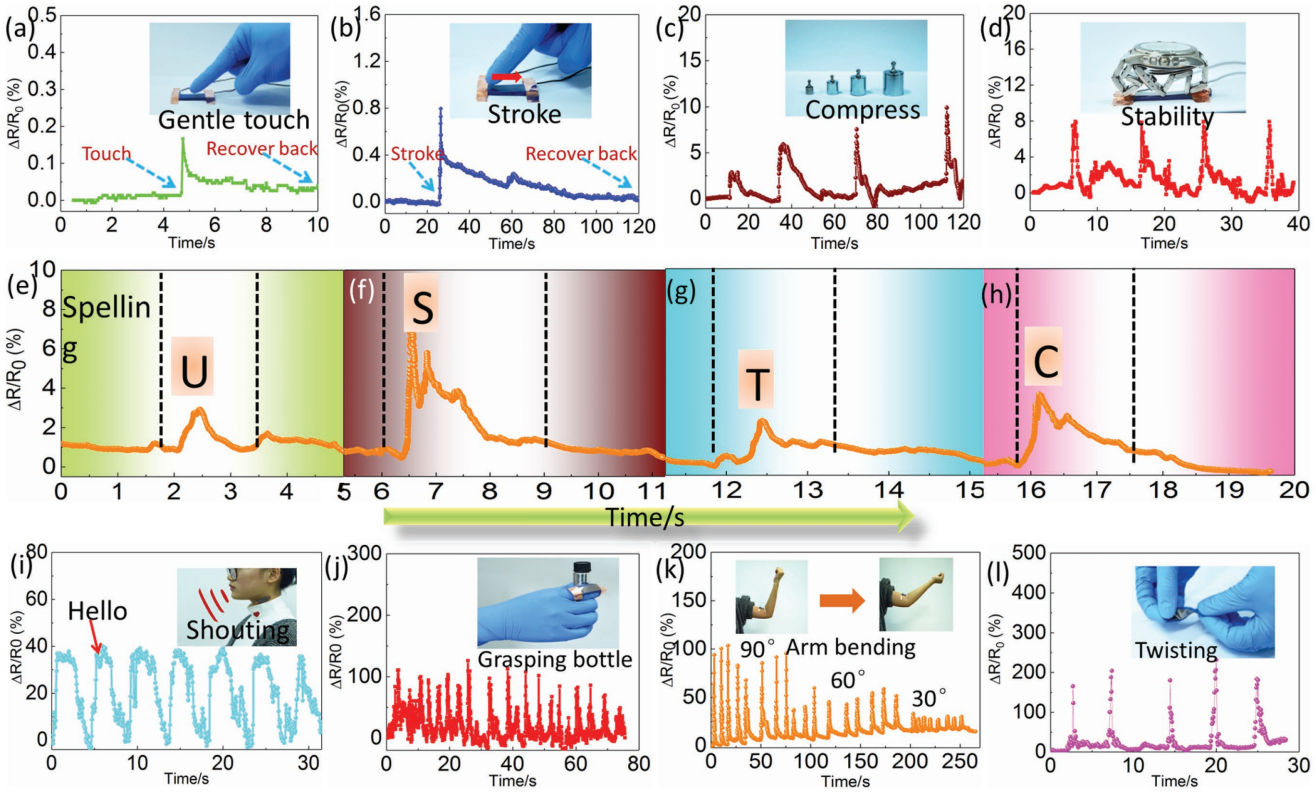

Figure 5. Tactile-perception behavior of e-skin by a) gentle touch, b) stroke, c,d) compression with reliability; e–h) spelling "USTC" and i) shouting; j) grasping, k) arm bending, l) and twisting.

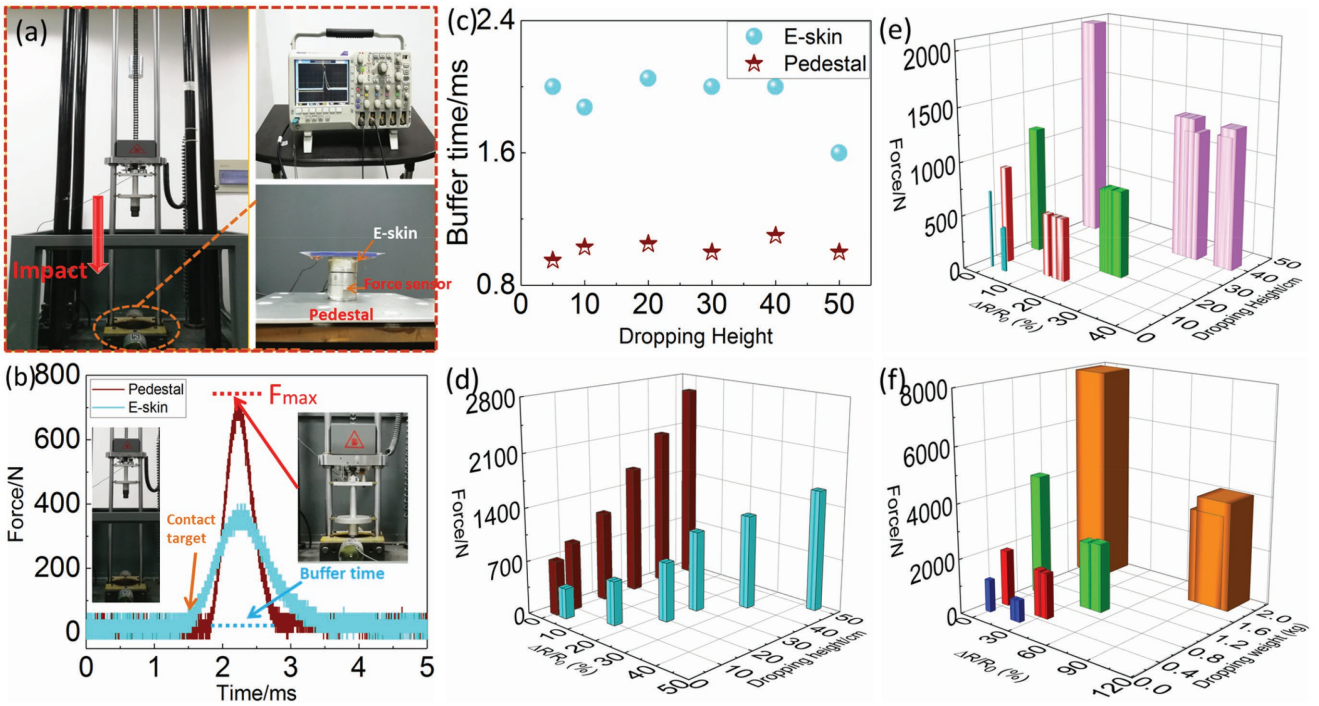

Figure 6. Tactile sensing and safeguarding performance of e-skin in drop hammer impact experiments: a) drop hammer test equipment, b) typical force–time curves recorded by force transducer (dropping height and weight are 5 cm and 0.25 kg, respectively); c) buffer times versus dropping height, impact force, and electrical signals versus d) falling height in the 3D bar graph (red bar indicates the drop weight impact on the force transducer, blue bar represents the weight impact on e-skin); e) reliability of e-skin during cyclic loading–unloading impacts, f) safeguarding performance and electrical sensing of e-skin versus dropping weight at the falling height of 20 cm.

much impact energy is absorbed. In addition, the buffer time is invariably longer (increases from about 0.9 to 2 ms) which also indicates that the e-skin can effectively impede the impact and prevent external hurt (Figure 6c). Figure 6d shows the maximum impact force and electrical signals versus falling heights. Clearly, e-skin shows characteristic increment in impact sensing from 3.4% to 43.8% with the falling heights from 5 to 50 cm. Additionally, the maximum forces are improved with increasing of the falling heights, and also show a substantial increment in dissipating impact energy. Figure 6e illustrates the favorable electrical and safeguarding stability during cycles of impact, implying its long working life and good reliability. Keeping the falling height at 20 cm, e-skin also exhibits ideal sensing properties and safeguarding properties under the excitation of different dropping weights (Figure 6f). The maximum impact forces loaded on e-skin increase from 800 to 3460 N when the dropping weights change from 0.25 to 2 kg (the maximum forces loaded directly on the metal pedestal increase from 1180 to 7780 N). To this end, the reported e-skin with ideal force sensing and safeguarding performance guarantees its potential application in next-generation artificial intelligence and wearable devices.

2.4. Thermosensation Behavior

Due to the incorporation of thermochromic nanofillers, e-skin exhibits outstanding temperature-sensing performance (**Figure** 7a–e). The temperature-dependent color changes of thermochromic fillers are presented in Figure S4 (Supporting Information). Clearly, the color transformation temperatures of thermochromic red, blue, and black nanofillers are 16, 40, and 60 °C, respectively. e-Skin is placed on the top of a temperature control platform, and its color interestingly changes from amaranth (10 °C), wathet blue (15–20 °C) to blue (23–35 °C). Blue color fading starts at about 39 °C and finally turns to white at 55 °C, exhibiting ideal temperature responsive property. The visible color variations can be used to assess external temperatures. Additionally, the temperature-dependent electrical (Figure 7f–j) and rheological (Figure 7k) properties are also investigated. The resistance shows three stages in 6–66 °C. At low temperature (lower than 11 °C), the resistance is about 4.2 Ω. It keeps at about 4.7 Ω in the range of 15–50 °C. When external temperature is higher than 54 °C, the resistance increases to 5.0 Ω. The electrical stability is mainly due to the protection from PET film and hybrid polymer. Polymer matrix which is strongly adhered on PET film in the curing process can prevent AgNWs against oxidation and water corrosion even at high temperature.[39,40] The storage modulus of e-skin shows inconspicuous decrement with increasing temperature (Figure 7k), indicating its stable mechanical performance in the range of 8–63 °C. To further investigate the ability against corrosion and oxidation, a long-term detection test for resistance of e-skin was conducted. Even after the 18 d, the resistance only increased about 13.7% which indicated the hierarchical structures of PET, and hybrid polymer could sufficiently protect AgNWs from corrosion and oxidation (Figure 7l). In conclusion, e-skin shows interesting thermal responsive performance, in which the environment temperature as well as electrical resistance can be assessed and detected by e-skin colors.

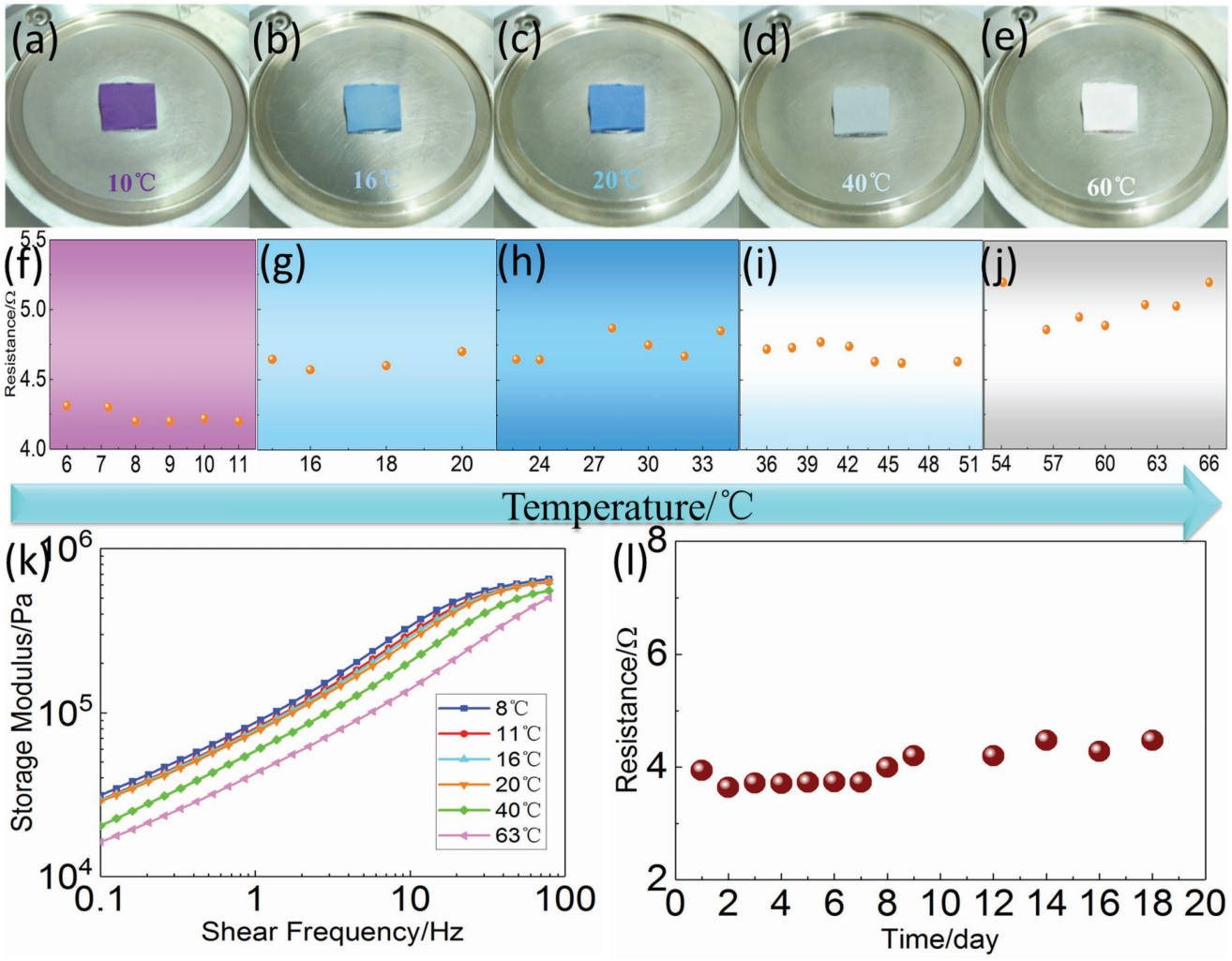

Figure 7. Schematic of sensing temperature changes of e-skin: a–e) temperature-dependent e-skin colors as epidermis from 10 to 60 °C and f–j) the corresponding resistance variation; k) temperature-dependent mechanical properties; and l) long-term stability of e-skin.

2.5. Flexible e-Skin Array Pad

Finally, a flexible sensor array pad with a 3 × 3 unit and 25 × 25 mm^2 spatial resolution was fabricated (**Figure 8**d) to study the precise emulating functions of e-skin. AgNWs/PET films were linked by conductive copper tape (Figure 8a), and the hybrid polymer was covered on the film and curried in a mold. The pressure mappings at different bending and quasistatic compression excitations are presented. Figure 8c shows the typical readable electrical mappings, and it is consistent with the actual pressure distribution by bending.[41] The array also monitors the position and detects the weight distribution by changing the pixel resistance under quasistatic compression (Figure 8f). In addition, an array of configurations of 1 pixel with a 15 × 15 mm^2 spatial resolution surrounded by 8 pixels (neighboring distance was 12 mm) was also designed to further investigate the force distribution and safeguarding performance when a harsh impact was loaded on the array (Figure 8g). Nine force sensors with the same configuration were fixed under the e-skin array to record the impact force (Figure S5b, Supporting Information). The sensor unit in the center recorded the maximum force as 995 N. Other force signals could not be clearly revealed in Figure 8h due to the lower values (the maximum force was lower than 32 N; Figure S5c, Supporting Information), which indicated that the impact force can be dissipated by the hybrid polymer effectively. Simultaneously, the pixel electrical resistance signals can map the impact locations precisely. It also reveals the amplitude and distribution of impact force. To this end, the flexible e-skin array is suitable for monitoring pressure distributions as well as protecting human beings under various conditions.

3. Conclusion

In this work, a novel e-skin array with multifunctional sensing properties and safeguarding performance was designed by assembling PET film, AgNWs, and hybrid polymer composites. Shear stiffening polymer mixed with small amounts of PDMS was used to prepare the hybrid polymer. The

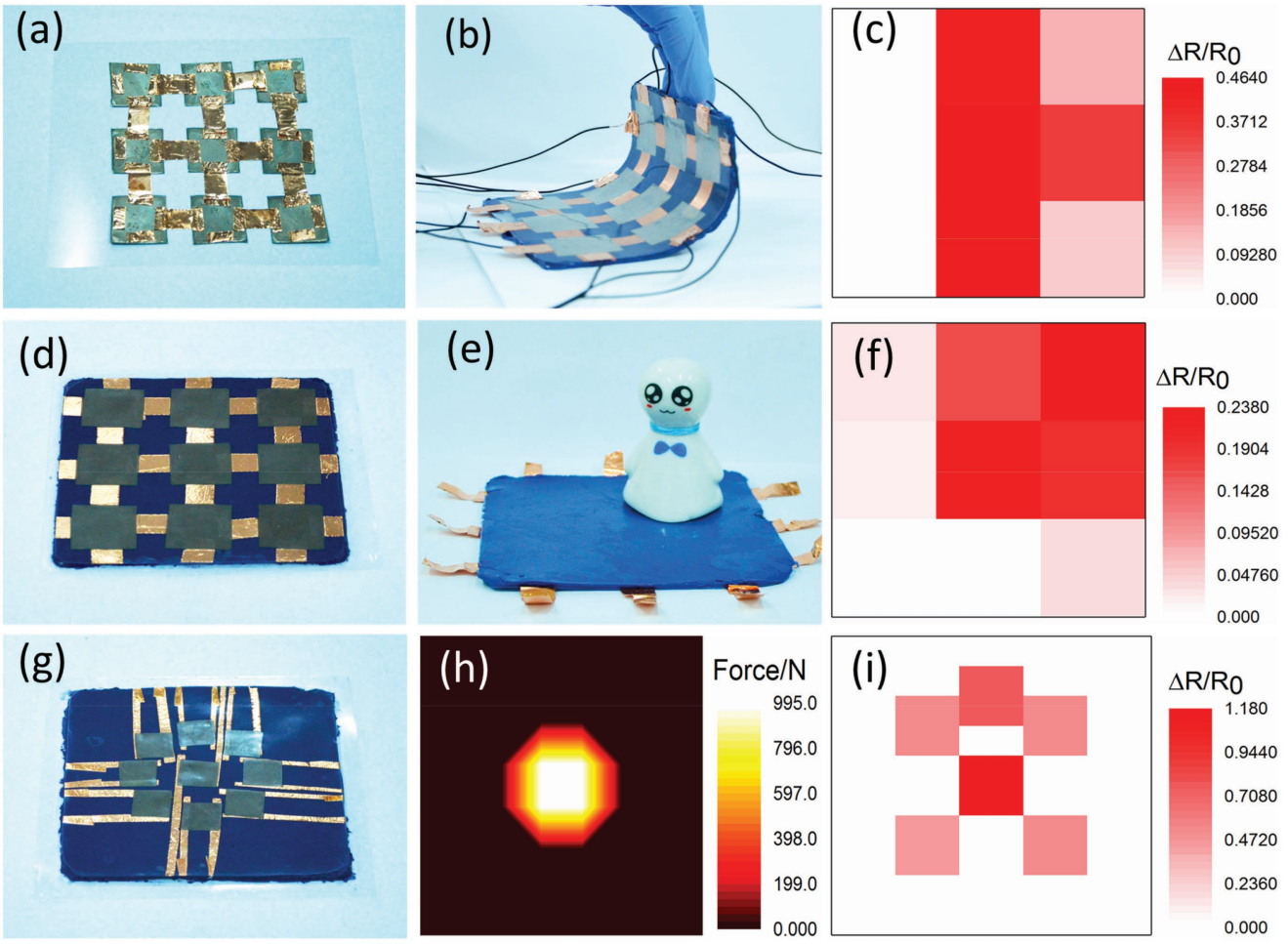

Figure 8. Photograph of 3 × 3 e-skin array: a) the array of Ag nanowires/polyester (AgNWs/PET) film as conductive array, b,c) recognition of the pressure distribution under bending, and d–f) quasistatic compressing excitation; h) dynamic impact force and i) resistance variation distribution by drop hammer impact experiment.

mechanical properties of e-skin show rate-dependent characteristic in which the G' can increase from 5.5 kPa to 0.39 MPa as the shear frequency varies from 0.1 to 100 Hz. e-Skin also exhibits multiple force sensing properties which can perceive bending, compressing, and twisting, as well as monitoring various human motions. The thermosensation ability of e-skin by varying the colors just like the chameleon epidermis can be used to assess external temperature. Moreover, e-skin with good shear stiffening property can impede external force and absorb nearly 50% of impact energy which presents ideal safeguarding property. The e-skin mapping array exhibits typical force and resistance distribution which demonstrates the high potential for monitoring human interactions, personal movement, environmental changes and safeguards.

4. Experimental Section

Synthesis of AgNW Solution: Briefly, polyvinyl pyrrolidone (5.86 g, $M_W \approx 40\,000$) was dissolved into glycerol (190 mL) at 90 °C by stirring and after cooling to 50 °C. $AgNO_3$ powder (1.58 g) was added. Then a solution containing glycerol (10 mL), NaCl (59 mg), and distilled (DI) water (0.5 mL) was poured into the flask by continuously stirring and heating. The gray–green solution was pulled into beakers when the reaction temperature reached to 210 °C. DI water (200 mL) was then added to the solution after it cooled to 90 °C. The mixture was placed 1 week followed by centrifuging, washing with DI water and ethanol each for three times. Finally, AgNWs were suspended in ethanol to form the AgNW solution.

Preparation of Artificial e-Skin: SST polymer was obtained by synthesizing a mixture of dimethyl siloxane, boric acid, and ethanol (with a mass ration of 15:2:1) at 220 °C for several hours. Then, SST polymer with HTV silicone rubber (MVQ 110–2, bought from Dong Jue Fine Chemicals Nanjing Co., Ltd) and BPO were homogeneously blended by a two-roll miller (Taihu Rubber Machinery Inc., China, Type XK-160) followed by addition of the commercially available thermochromic fillers (bought from Shenzheng Bianse Chemical Technology Co., Ltd, China). The mass ratio of thermochromic red, blue, and black fillers was 10:2:1. The above AgNW solution was dipped dropwise on PET film to form conductive AgNW layer, and copper foil was fixed at the ends of film. Finally, conductive PET film was placed on a steel mold, covered by the SST/PDMS polymer composite, and they were cured by a plate vulcanizing apparatus (Model: BL-6170-B) at 90 °C under 20 MPa for 15 min. After cooling down, the final artificial e-skin was acquired by adhering copper wire on copper foil electrodes.

Characterization of the e-Skin: The micromorphologies of the as-prepared e-skin were characterized by SEM (GeminiSEM 500, ZEISS). XRD patterns of hybrid polymer composites were analyzed by an X-ray diffractometer (SmartLab 9 kW). The FT-IR spectrum was measured by a Nicolet Model 8700 Fourier transform infrared

spectrometer in the range of 4000–550 cm^{-1}. The rheological properties were studied by a rheometer (Physica MCR 301, Anton Paar Co., Austria). Samples were molded into a cylinder with the thickness and diameter of 1 and 20 mm, respectively. The shear frequency was ranged from 0.1 to 100 Hz and the strain was kept at 0.1%. The electrical performance was measured by an EIS system which was equipped with a Modulab material test system and data storage unit. Additionally, the safeguarding properties of the artificial skin were further investigated by a drop hammer test system.

Supporting Information

Supporting Information is available from the Wiley Online Library or from the author.

Acknowledgements

S.W. and L.G. contributed equally to this work. Financial supports from the National Natural Science Foundation of China (Grant Nos. 11772320 and 11372301), the Strategic Priority Research Program of the Chinese Academy of Sciences (Grant No. XDB22040502), and the Fundamental Research Funds for the Central Universities (WK2480000002) are gratefully acknowledged. This study was also supported by the Collaborative Innovation Center of Suzhou Nano Science and Technology.

Conflict of Interest

The authors declare no conflict of interest.

Keywords

artificial electrical skin, force sensing, hybrid structures, safeguarding performance, thermosensation

Received: December 28, 2017
Revised: January 28, 2018
Published online: March 1, 2018

[1] S. Naik, N. Bouladoux, J. L. Linehan, S. J. Han, O. J. Harrison, C. Wilhelm, S. Conlan, S. Himmelfarb, A. L. Byrd, C. Deming, M. Quinones, J. M. Brenchley, H. H. Kong, R. Tussiwand, K. M. Murphy, M. Merad, J. A. Segre, Y. Belkaid, *Nature* **2015**, *520*, 104.
[2] J. Oh, A. L. Byrd, M. Park, H. H. Kong, J. A. Segre, *Cell* **2016**, *165*, 854.
[3] C. C. Kim, H. H. Lee, K. H. Oh, J. Y. Sun, *Science* **2016**, *353*, 682.
[4] J. Ge, H. B. Yao, X. Wang, Y. D. Ye, J. L. Wang, Z. Y. Wu, J. W. Liu, F. J. Fan, H. L. Gao, C. L. Zhang, S. H. Yu, *Angew. Chem., Int. Ed.* **2013**, *52*, 1654.
[5] H. F. Zhu, X. W. Wang, J. Liang, H. L. Lv, H. Y. Tong, L. B. Ma, Y. Hu, G. Y. Zhu, T. Zhang, Z. X. Tie, Z. Liu, Q. W. Li, L. W. Chen, J. Liu, Z. Jin, *Adv. Funct. Mater.* **2017**, *27*, 1606604.
[6] C. Pang, G. Lee, T. Kim, S. M. Kim, H. N. Kim, S. H. Ahn, K. Y. Suh, *Nat. Mater.* **2012**, *11*, 795.
[7] H. B. Yao, J. Ge, C. F. Wang, X. Wang, W. Hu, Z. J. Zheng, Y. Ni, S. H. Yu, *Adv. Mater.* **2013**, *25*, 6692.
[8] B. C. Tee, C. Wang, R. Allen, Z. Bao, *Nat. Nanotechnol.* **2012**, *7*, 825.
[9] Z. F. Liu, S. Fang, F. A. Moura, J. N. Ding, N. Jiang, J. Di, M. Zhang, X. Lepró, D. S. Galvão, C. S. Haines, N. Y. Yuan, S. G. Yin, D. W. Lee, R. Wang, H. Y. Wang, W. Lv, C. Dong, R. C. Zhang, M. J. Chen, Q. Yin, Y. T. Chong, R. Zhang, X. Wang, M. D. Lima, R. Ovalle-Robles, D. Qian, H. Lu, R. H. Baughman, *Science* **2015**, *6246*, 400.
[10] J. Park, Y. Lee, J. Hong, M. Ha, Y. D. Jung, H. Lim, S. Y. Kim, H. Ko, *ACS Nano* **2014**, *5*, 4689.
[11] F. R. Fan, L. Lin, G. Zhu, W. Z. Wu, R. Zhang, Z. L. Wang, *Nano Lett.* **2012**, *6*, 3109.
[12] G. Zhu, W. Q. Yang, T. J. Zhang, Q. S. Jing, J. Chen, Y. S. Zhou, P. Bai, Z. L. Wang, *Nano Lett.* **2014**, *14*, 3208.
[13] C. Dagdeviren, Y. Su, P. Joe, R. Yona, Y. Liu, Y. S. Kim, Y. A. Huang, A. R. Damadoran, J. Xia, L. W. Martin, Y. G. Huang, J. A. Rogers, *Nat. Commun.* **2014**, *5*, 4496.
[14] Q. Z. Zhong, J. W. Zhong, X. F. Cheng, X. Y, B. Wang, W. B. Li, N. Wu, K. Liu, B. Hu, J. Zhou, *Adv. Mater.* **2015**, *27*, 7130.
[15] M. Q. Jian, K. L. Xia, Q. Wang, Z. Yin, H. M. Wang, C. Y. Wang, H. H. Xie, M. C. Zhang, Y. Y. Zhang, *Adv. Funct. Mater.* **2017**, *27*, 1606066.
[16] W. T. Cai, Y. Huang, D. Y. Wang, C. X. Liu, Y. G. Zhang, *J. Appl. Polym. Sci.* **2014**, *131*, 39778.
[17] F. Deng, M. Ito, T. Noguchi, L. F. Wang, H. Ueki, K. I. Niihara, Y. A. Kim, M. Endo, Q. S. Zheng, *ACS Nano* **2011**, *5*, 3858.
[18] Z. M. Dang, M. J. Jiang, D. Xie, S. H. Yao, L. Q. Zhang, J. B. Bai, *J. Appl. Phys.* **2008**, *104*, 024114.
[19] S. F. Zhao, J. H. Li, D. X. Cao, G. P. Zhang, J. Li, K. Li, Y. Yang, W. Wang, Y. F. Jin, R. Sun, C. P. Wong, *ACS Appl. Mater. Interfaces* **2017**, *9*, 12147.
[20] X. X. Yin, T. P. Vinod, R. Jelinek, *J. Mater. Chem. C.* **2015**, *3*, 9247.
[21] Q. Wang, M. Q. Jian, C. Y. Wang, Y. Y. Zhang, *Adv. Funct. Mater.* **2017**, *27*, 1605657.
[22] D. H. Ho, Q. J. Sun, S. Y. Kim, J. T. Han, D. H. Kim, J. H. Cho, *Adv. Mater.* **2016**, *28*, 2601.
[23] C. Y. Hou, T. Huang, H. Z. Wang, H. Yu, Q. H. Zhang, Y. G. Li, *Sci. Rep.* **2013**, *3*, 3138.
[24] C. G. Núñez, W. T. Navaraj, E. O. Polat, R. Dahiya, *Adv. Funct. Mater.* **2017**, *27*, 1606287.
[25] Y. L. Tai, T. Chen, G. Lubineau, *ACS Appl. Mater. Interfaces* **2017**, *9*, 32184.
[26] Z. J. Fan, B. Liu, J. Q. Wang, S. Y. Zhang, Q. Q. Lin, P. W. Gong, L. M. Ma, S. R. Yang, *Adv. Funct. Mater.* **2014**, *24*, 3933.
[27] W. Sheng, J. W. Quan, J. W. Feng, Y. Fang, M. Ya, X. S. Hu, G. X. Long, *J. Mater. Chem. C* **2014**, *2*, 7133.
[28] F. Guo, C. B. Du, G. J. Yu, R. P. Li, *Adv. Mater. Sci. Eng.* **2016**, *10*, 7079698.
[29] S. Wang, S. H. Xuan, W. Q. Jiang, W. F. Jiang, L. X. Yan, Y. Mao, M. Liu, X. L. Gong, *J. Mater. Chem. A* **2015**, *3*, 19790.
[30] S. Wang, S. H. Xuan, M. Liu, L. F. Bai, S. S. Zhang, M. Sang, W. Q. Jiang, X. L. Gong, *Soft Matter* **2017**, *13*, 2483.
[31] K. Liu, A. Pei, H. R. Lee, B. Kong, N. Liu, D. C. Lin, Y. Y. Liu, C. Liu, P. C. Hsu, Z. N. Bao, Y. Cui, *J. Am. Chem. Soc.* **2017**, *139*, 4815.
[32] C. S. Boland, U. Khan, G. Ryan, S. Barwich, R. Charifou, A. Harvey, C. Backs, Z. L. Li, M. S. Ferreira, M. E. Mobius, R. J. Young, J. N. Coleman, *Science* **2016**, *354*, 1257.
[33] S. Wang, S. H. Xuan, Y. P. Wang, C. H. Xu, Y. Mao, M. Liu, L. F. Bai, W. Q. Jiang, X. L. Gong, *ACS Appl. Mater. Interfaces* **2016**, *8*, 4946.
[34] Y. Q. Jiang, J. Xi, Z. X. Wu, H. Dong, Z. X. Zhao, B. Jiao, X. Hou, *Langmuir* **2015**, *31*, 4950.
[35] M. X. Jing, M. Li, C. Y. Chen, Z. Wang, X. Q. Shen, *J. Mater. Sci.* **2015**, *50*, 6437.
[36] T. Tokuno, M. Nogi, M. Karakawa, J. T. Jiu, T. T. Nge, Y. Aso, K. Suganuma, *Nano Res.* **2011**, *4*, 1215.
[37] L. Jinhwan, L. Phillip, L. H. Beom, H. Sukioon, L. Inhwa, Y. Junyeob, L. S. Seob, K. T. Soo, L. D. Jin, K. S. Hwan, *Adv. Funct. Mater.* **2013**, *23*, 4171.
[38] F. Xu, Y. Zhu, *Adv. Mater.* **2012**, *24*, 5117.
[39] D. S. Ghosh, T. L. Chen, V. Mkhitaryan, V. Pruneri, *ACS Appl. Mater. Interfaces* **2014**, *6*, 20943.
[40] H. G. Im, J. Jin, J. H. Ko, J. Lee, J. Y. Lee, B. S. Bae, *Nanoscale* **2014**, *6*, 711.
[41] Y. L. Tai, Z. G. Yang, *J. Mater. Chem. B* **2015**, *3*, 5436.

